Detailed simulation of turbulent flow within a suction and oscillatory blowing fluidic actuator

By J. Kim AND P. Moin

1. Motivation and objectives

Fluidic actuators have been widely used for several decades to control turbulent flows. Although their application and objectives vary depending on the particular configurations of turbulent flows and actuator types, the basic mechanism of fluidic actuators is the same: adding or removing fluid momentum to perturb, at least, the local state of the flow so that an integral quantity of interest (for example, skin friction, drag coefficients, overall sound pressure level) is improved. Several types of fluidic actuators can be found with their mechanisms based upon, for example, steady suction, blowing and suction with zero-net mass flux, resonance, or synthetic jet (Gad-el Hak 2000; Greenblatt & Wygnanski 2000; Collis *et al.* 2004; Cattafesta III & Sheplak 2011; Mohseni & Mittal 2014).

Recently, a novel fluidic actuator using steady suction and oscillatory blowing was developed for the active control of high-speed turbulent flows (Arwatz *et al.* 2008). The concepts of suction and oscillatory blowing are integrated into a single active control device for higher control authority. The actuation is based upon a self-sustained mechanism of unsteady flows and does not require any moving parts. The output is controlled primarily by its pressure source and the feedback tube (discussed in Section 2), and no additional input is needed. This new fluidic actuator demonstrates a robust and effective performance for delaying boundary-layer separation and bluff-body drag reduction.

The internal flow in this actuator has been subject to detailed examination in an effort to quantify the actuator's behavior as well as to develop a predictive model for the actuation (Arwatz *et al.* 2008; Wassermann *et al.* 2013). Arad (2014) conducted both unsteady Reynolds Averaged Navier–Stokes (URANS) and incompressible large eddy simulation (LES) using the same grid. It was argued that URANS could predict the oscillatory jet based upon the observation that a key contributing factor to jet oscillation is the Coandă effect, which is not strongly turbulent motion. Although LES was able to reproduce some of the important features of the oscillatory jet within the actuator, the oscillatory behavior was not quite clear for the URANS results. Both calculations demonstrated some discrepancy with the experimental measurements. Several inconsistencies were pointed out for LES, such as using an incompressible flow solver, neglecting the suction box, and prescribing steady suction as a boundary condition.

In this study, a high-fidelity simulation of the internal jet flow within the fluidic actuator is performed. A fully compressible LES solver is used and a complete geometry of the actuator is simulated. In Section 2, the Suction and Oscillatory Blowing actuator is described. Computational conditions are discussed in Section 3, followed by simulation results in Section 4. The report concludes with a summary and outlook for future work in Section 5.

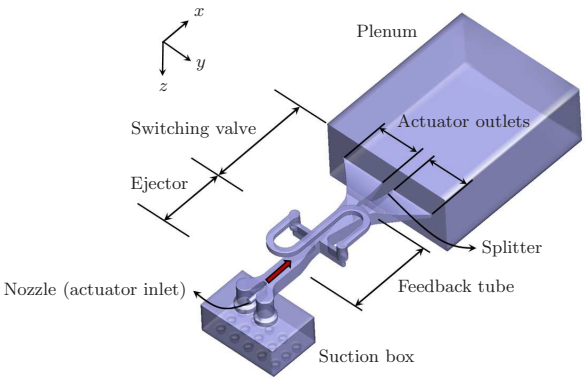

FIGURE 1. The SaOB fluidic actuator. The block arrow indicates the main flow direction.

2. Suction and Oscillatory Blowing (SaOB) fluidic actuator

In this section, the SaOB fluidic actuator and its operating mechanism are briefly explained. A more detailed description can be found in Arwatz *et al.* (2008).

The schematic diagram for the full-geometry SaOB fluidic actuator is shown in Figure 1. Throughout this report, x is the streamwise direction, y is the transverse direction, and z is the spanwise direction. The center-plane corresponds to $y = 0$ around which the actuator geometry is symmetric, except for the feedback tube. A pressure source such as a stagnation chamber is connected to the converging nozzle, and a round jet is injected into the ejector with a square cross section. The flow direction is given by the block arrow in Figure 1. The suction box connected to the atmospheric or lower-pressure air supplies an appropriate amount of entrainment through the holes on the suction-box surface. The suction box is connected to the ejector via two suction ports. The amount of suction is dynamically determined by the pressure condition within the ejector, which determines the total flow rate of the actuator. The round jet develops within the ejector and enters the switching valve after a mildly converging section. The switching valve has two actuator outlets (top and bottom for $y > 0$ and $y < 0$, respectively) downstream of the splitter. The S-shaped feedback tube connects the upper and lower pressure ports and is essential for the self-sustained operation of the actuator.

Under certain operating conditions, the plane jet within the switching valve oscillates in time. First, the jet loses symmetry with respect to $y = 0$, presumably due to the amplified unstable modes of the plane jet. Then, it deflects to one side and eventually attaches to the corresponding wall in y direction. A transverse pressure gradient caused by the Coandă effect (Tritton 1986) pushes the jet close to the wall and the jet eventually attaches to the wall. Without the feedback tube, the wall-attached jet is stable in time and does not oscillate. However, the presence of the feedback tube enables momentum transfer from one side of the pressure ports to the other. The momentum is driven by the pressure difference between the two pressure ports. The pressure port on the side where the jet is deflected has lower pressure due to the local acceleration caused by the Coandă effect. Subsequently, pressure on the other side of the pressure port becomes relatively higher and momentum is transferred to the lower-pressure port. The resulting transverse pressure gradient competes with the Coandă force stabilzing the jet near the wall and eventually detaches the jet. Once detached from the wall and crossing $y = 0$, the jet moves quickly to the other side due to the cooperative effect between the transverse pressure gradient and the Coandă force. The wall-attached jet detaches in the same way

and re-attaches to the original side of the wall, thus completing a single oscillation cycle. The oscillation is repeated in a self-sustained manner at a certain frequency determined primarily by the length and cross-sectional area of the feedback tube, temperature within the tube, and the nozzle inlet pressure (Viets 1975; Raman *et al.* 1994).

The SaOB fluidic actuator is robust and effective in providing high-speed, bi-stable oscillatory blowing at a prescribed frequency by the self-sustained mechanism. An important characteristic of the actuator is that none of its components move to produce the oscillatory blowing and no additional input is needed to sustain the oscillation; the main control input is the nozzle inlet pressure, which determines the overall flow rate of the actuator. Another advantage is the amplification of the flow rate caused by the low-pressure cavity formed within the switching valve when the jet is attached to one side of the walls. The low-pressure zone entrains fluid outside of the actuator outlet and increases the amount of blowing. Its high control authority is promising in actively controlling turbulent flows. Wilson *et al.* (2013) applied an array of 28 SaOB actuators synchronized in phase to delay boundary-layer separation and reduce the drag of an axisymmetric body. Its effectiveness as an active flow control device is demonstrated experimentally for canonical flow configurations (Wilson *et al.* 2013; Shtendel & Seifert 2014).

3. Computational conditions

The high-fidelity, computational fluid dynamics code, CharLES†, is used to solve the fully compressible Navier–Stokes equations. The governing equations are non-dimensionalized by the nozzle radius $r_j = D_j/2$, the ambient speed of sound c_∞, density ρ_∞, temperature T_∞, and molecular viscosity μ_∞, where the subscript ∞ denotes the ambient state. The ideal gas is assumed with $\gamma = c_p/c_v = 1.4$, where c_p and c_v are the specific heats at a constant pressure and volume, respectively. The viscosity is assumed to be a function of temperature only and to follow the power-law relation, $\mu/\mu_\infty = (T/T_\infty)^n$ where $n = 0.76$. The Reynolds number based on the nozzle-exit condition (denoted by the subscript j) is $Re_j = \rho_j u_j D_j/\mu_j = 64000$ and the Prandtl number is assumed constant as $Pr = 0.7$. The subgrid-scale model of Vreman (2004) is used with the model constant $c = 0.07$ and the constant turbulent Prandtl number $Pr_t = 0.9$.

The governing equations are discretized in space using the cell-based finite volume formulation. The solutions are time advanced using the standard third-order Runge–Kutta method at a constant (non-dimensional) time-step size of $\Delta t = 0.00075$, which results in the Courant–Friedrichs–Lewy number of approximately 1.0. The spatial discretization is non-dissipative and formally second-order accurate on arbitrary unstructured grids. In addition, the convective fluxes are combined, depending on local grid quality (for example, element skewness), with fluxes computed by an HLLC-upwind discretization. Khalighi *et al.* (2011) provide more detailed discussions on the spatial discretization.

A base grid of 19 million unstructured control volumes is generated and subsequently refined using Adapt, the grid-adapting tool in the CharLES suites. For computational accuracy and efficiency, only hexahedral elements are used. The total number of control volumes for the adapted grid is 37 million. A cross-section of the computational grid is shown in Figure 2.

The nozzle is supplied with air at 24 psi, and its total temperature is the same as the ambient temperature. The Mach number at the nozzle exit is $\mathrm{M}_j = u_j/c_j = 0.87$. The

† http://www.cascadetechnologies.com/pdf/CHARLES.pdf

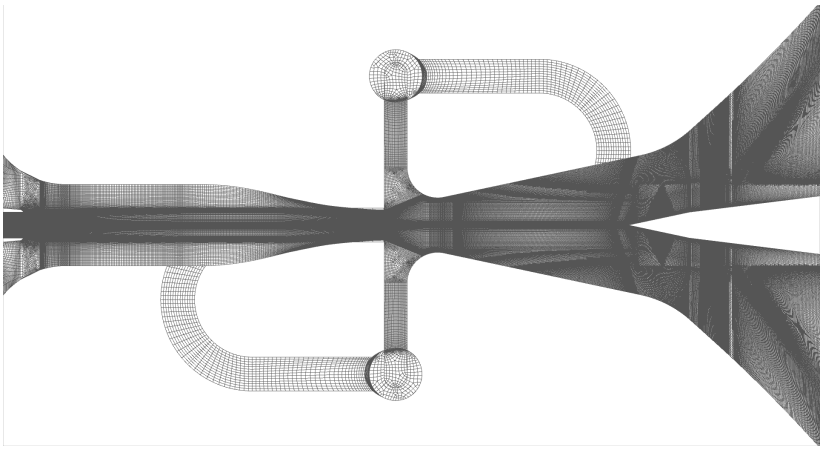

FIGURE 2. The computational grid for the ejector and switching valve.

suction holes and the plenum outlet are at the ambient condition. The no-slip solid wall boundaries are modeled isothermally at the ambient temperature.

The simulation is performed in the ALCF Mira cluster using 8,192 cores. There are approximately 4,500 control volumes per core, and the code scales very well up to this number of cores.

4. Results

4.1. *Self-sustained oscillation of the ejector jet*

The flow within the SaOB actuator is time advanced until initial transients are swept away and the jet in the switching valve establishes a bi-stable oscillation. To initiate an oscillatory state, steady suction is applied on the upper wall of the switching valve ($y > 0$) until the jet attaches to it, after which the wall is switched back to a no-slip and no-penetration solid wall. The oscillation frequency $f_0 = 1/T_0$ is estimated based upon the time history of the volume flow rate on the actuator outlets shown in Figure 3. The current simulation predicts the switching frequency to be 243 Hz, while the experiment measures 211 Hz under the corresponding inlet pressure. The oscillation frequency can also be estimated by calculating the volume flow rates on the pressure ports, as shown in Figure 4(a). The volume flow rates can be accurately modeled by a sinusoidal function with a constant period superimposed by high-frequency fluctuations. The lower and upper pressure ports are synchronous and in-phase in time, consistent with the measurements (Arwatz *et al.* 2008). Note that the measured frequency in the experiments is not constant but fluctuates over the oscillation periods by about 10 Hz, presumably due to strong turbulent fluctuations within the switching valve.

The first column of Figure 5 shows the instantaneous velocity contours on $z = 0$ at different phases of the oscillation. The jet demonstrates an apparent switching between the upper and lower sections of the switching valve. Large-scale instability wave-like structures are clearly seen. Note that t^* in Figure 5 is same as t^* in Figure 3. In the second column, instantaneous velocity magnitudes on the actuator outlets are shown at each phase of the oscillation. The outlet to which the jet is deflected has the maximum velocity of ~ 0.28. On the other side, the instantaneous velocity is approximately uniform in the transverse direction with a magnitude of 20% to 40% of the maximum velocity.

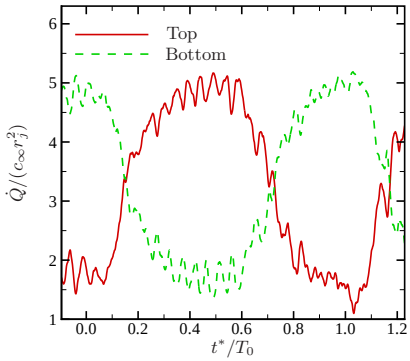

FIGURE 3. Volume flow rates on the top and bottom sides of the actuator outlets. The horizontal axis is the relative time with its reference defined in Figure 5(a). The oscillation period is denoted by T_0.

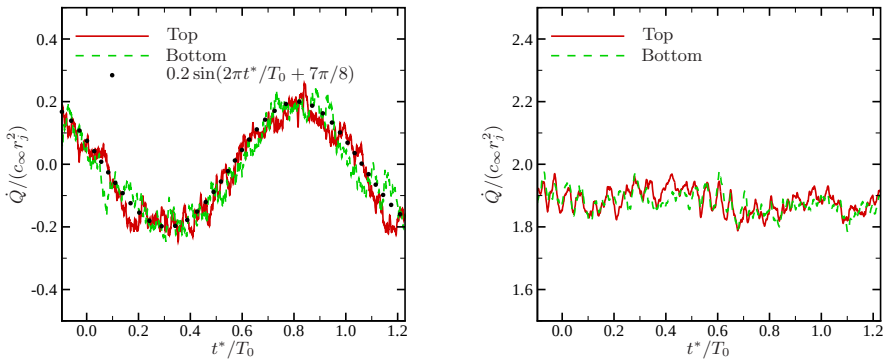

FIGURE 4. Volume flow rates on the top and bottom sides of (a) the pressure ports and (b) the suction ports. The horizontal axis is the relative time with its reference defined in Figure 5(a). The oscillation period is denoted by T_0.

4.2. *Statistics*

The solutions are time averaged and statistics are compared with the corresponding experiment. Due to the substantially low non-dimensional frequency ($f_0 r_j/c_\infty = 9.8 \times 10^{-4}$), statistical samples are collected only for a single oscillation period; additional simulations will be performed to obtain converged statistics for several oscillation periods.

The quantity of particular interest for this actuator is the velocity at the actuator outlet. In Figure 6(a), contours of time-averaged streamwise velocity are shown. The locations of maximum velocity lie close to the splitter wall. Figure 6(b) shows time-averaged velocities at the spanwise centerline on the actuator outlet. For plotting purposes, the sign of the y-velocity profile in the bottom side of the outlet is switched for comparison with the profile in the upper side. The profiles are fairly symmetric and the maximum streamwise velocity is 0.16, corresponding to 56 m/s. The experiment reports a maximum velocity of 44 m/s, a 27% error compared to the current prediction.

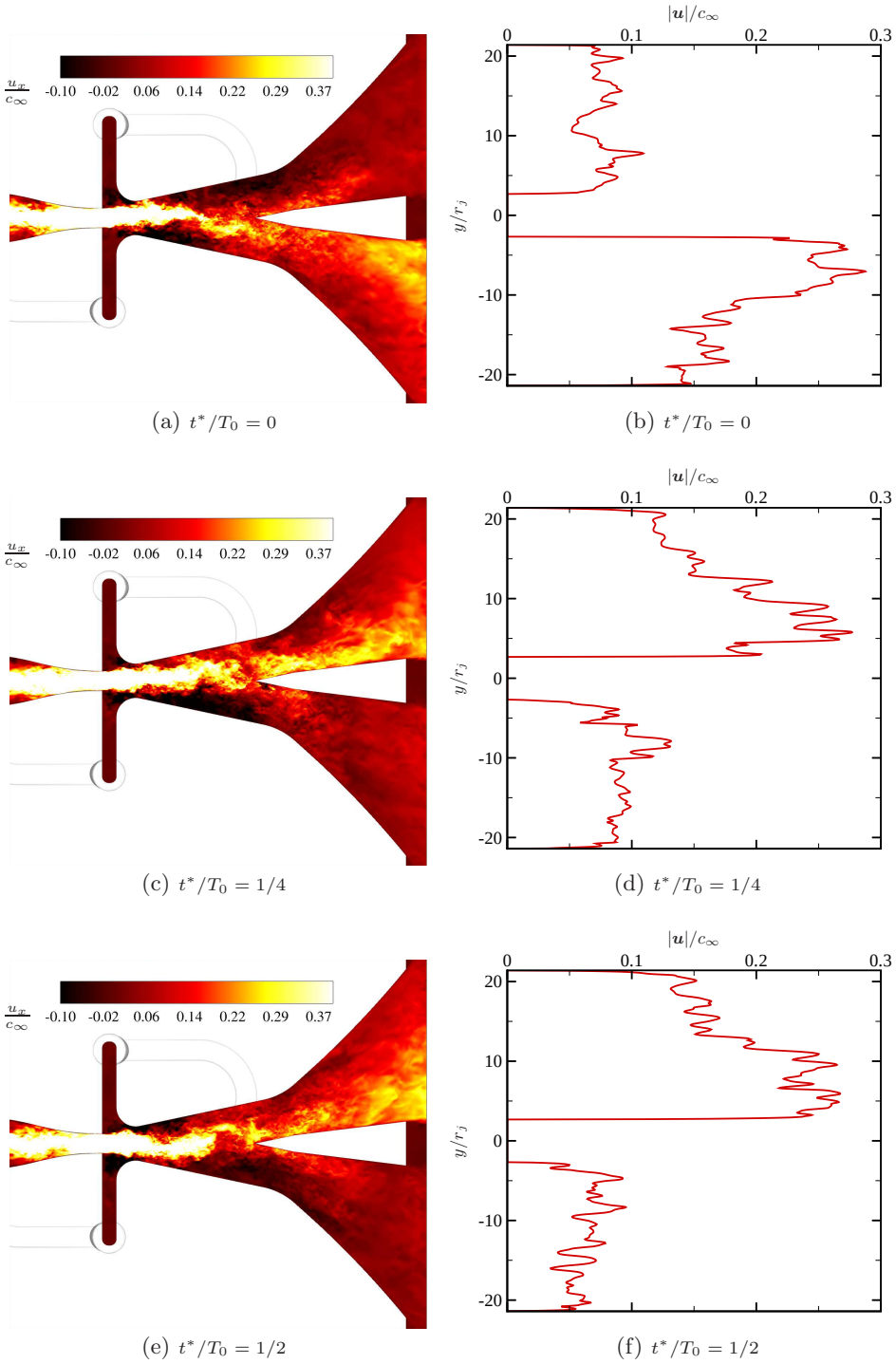

(a) $t^*/T_0 = 0$ (b) $t^*/T_0 = 0$

(c) $t^*/T_0 = 1/4$ (d) $t^*/T_0 = 1/4$

(e) $t^*/T_0 = 1/2$ (f) $t^*/T_0 = 1/2$

FIGURE 5. For the caption, see the next page.

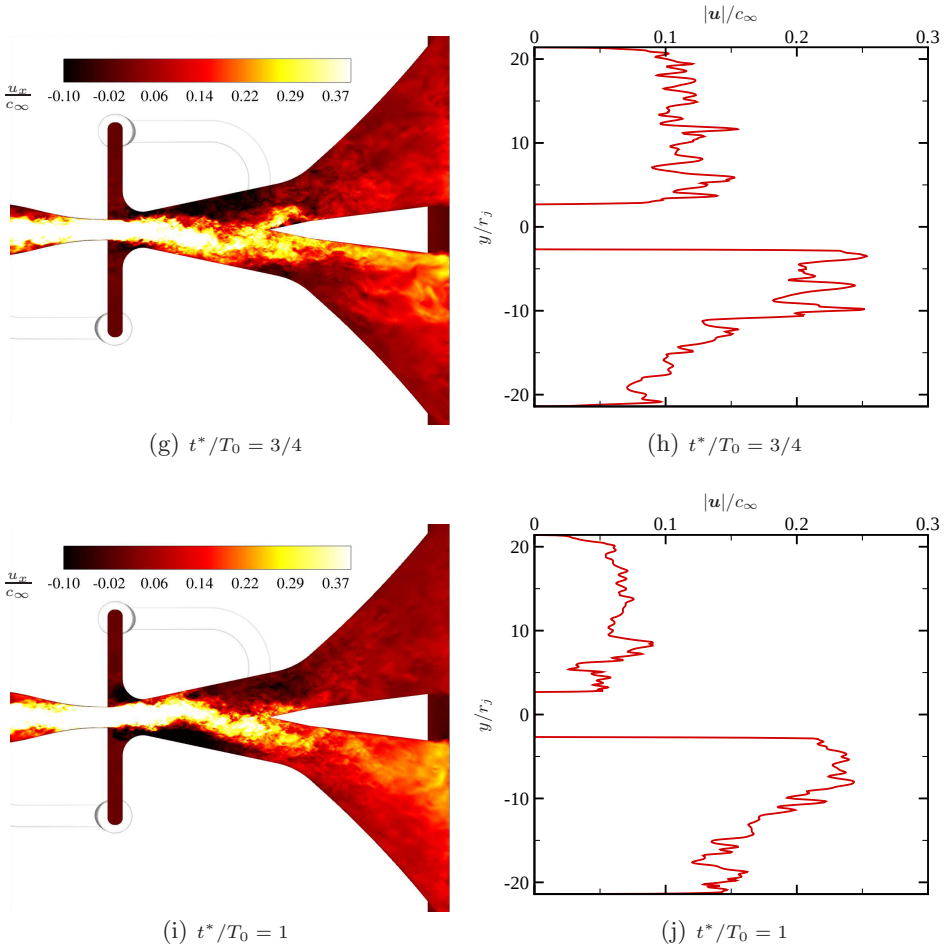

FIGURE 5. Instantaneous contours of streamwise velocity (left column) and transverse profiles of velocity magnitude (right column).

The suction box shown in Figure 1 entrains the ambient air into the ejector. The round jet within the ejector has static pressure lower than the ambient pressure. This causes a pressure difference between the ejector and the suction box connected to the ambient air. Thus, air is drawn into the suction box and flows into the ejector. In the previous computational study (Arad 2014), this entrainment was modeled as a boundary condition of a constant volume flow rate, which matches the corresponding experimental data in a time-averaged sense. The volume flow rates through the suction ports are shown in Figure 4(b) and the mean volume flow rate is 2.6×10^{-3} m^3/s. This is an approximately 25% underprediction of the experimental measurement.

The reduced entrainment is a consequence of a lower pressure difference between the ambient air and the ejector jet. The static pressure within the suction box is nearly uniform (within 0.2%) as the ambient pressure. This suggests that the pressure of the ejector jet is overpredicted. Another possibility is that turbulent mixing of the ejector jet is not as strong as in the experiment, resulting in less ambient air entrainment. For the present simulation, the spatial resolution within the ejector may have a strong

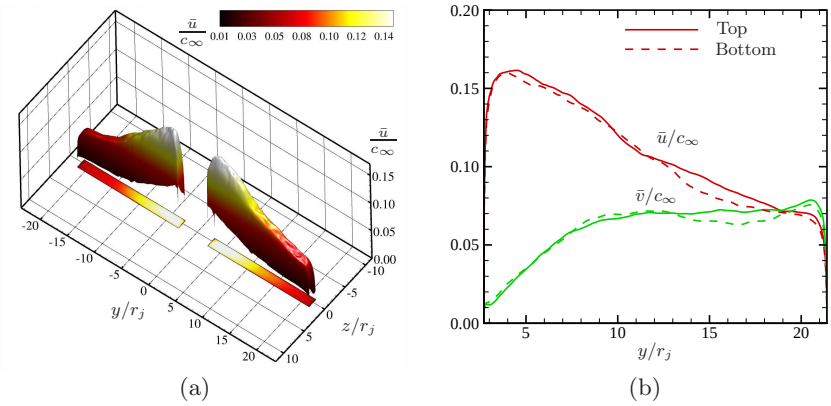

FIGURE 6. Time-averaged velocity on the actuator outlet: (a) streamwise velocity contour and (b) velocity profiles at $z = 0.2$.

impact on the development of the turbulent jet. Currently, the ejector grid is further refined and additional simulation is being performed to assess this hypothesis. In any case, the reduced entrainment is associated with a reduced growth rate of the jet in the streamwise direction. Consequently, the jet centerline velocity decays more slowly, and thus the velocity at the ejector exit becomes higher. The increased velocity at the ejector exit appears to result in higher frequency jet oscillations in the switching valve, which is consistent with the current observation and the experiment (Arwatz *et al.* 2008).

5. Summary and future work

Turbulent flow within the Suction and Oscillatory Blowing (SaOB) actuator is simulated. The SaOB fluidic actuator is developed to provide high-momentum oscillatory blowing for active flow control, such as separation delay of the high-speed boundary layer over airfoils. Its operating mechanism is based upon a balance between the transverse pressure gradient generated by the oscillating jet and the Coandă force, and it does not involve any moving parts. Its control authority has been demonstrated for several canonical flow configurations.

Providing detailed and reliable description of the unsteady internal flow is important for a better understanding of the physical mechanisms and eventually improving the actuator design. Large-eddy simulation technique is applied to compute the compressible turbulent flow within the actuator. The actuator geometry is represented using an adapted unstructured grid with 37 million control volumes.

The simulation predicts the time-dependent switching behavior of the turbulent jet. The oscillatory motion repeats in a self-sustained manner at a frequency close to the experimental measurement. Despite some quantitative discrepancies with the experiment, the preliminary results are encouraging. Simulations with more increased grid resolution using 280 million control volumes are underway. Additional simulations will be performed using inlet pressures of 5, 10, and 20 psi to parametrically assess the fidelity of the current prediction.

Acknowledgments

The primary computing resources were provided by the Argonne National Laboratory through the ASCR Leadership Computing Challenge. The authors also acknowledge National Science Foundation for supporting the Certainty cluster at the Center for Turbulence Research. Financial support from NASA and the Boeing Company is gratefully acknowledged. The authors would like to thank Prof. Avraham Seifert for providing the actuator geometry and engaging in valuable discussions. The first author is grateful to Dr. George Ilhwan Park, Dr. Yee Chee See, Ik Jang, and Brian Pierce for help in using the CharLES code and for useful discussions.

REFERENCES

Arad, E. 2014 The appropriate level of simulation for a fluidic oscillator AFC device (private communication) pp. 1–12.

Arwatz, G., Fono, I. & Seifert, A. 2008 Suction and oscillatory blowing actuator modeling and validation. *AIAA J.* **46**, 1107–1117.

Cattafesta III, L. N. & Sheplak, M. 2011 Actuators for active flow control. *Annu. Rev. Fluid Mech.* **43**, 247–272.

Collis, S. S., Joslin, R. D., Seifert, A. & Theofilis, V. 2004 Issues in active flow control: theory, control, simulation, and experiment. *Prog. Aerosp. Sci.* **40**, 237–289.

Greenblatt, D. & Wygnanski, I. J. 2000 The control of flow separation by periodic excitation. *Prog. Aerosp. Sci.* **36**, 487–545.

Gad-el Hak, M. 2000 *Flow Control: Passive, Active, and Reactive Flow Management*. Cambridge University Press.

Khalighi, Y., Nichols, J. W., Lele, S. K., Ham, F. & Moin, P. 2011 Unstructured large eddy simulation for prediction of noise issued from turbulent jets in various configurations. *AIAA Paper 2011–2886.*

Mohseni, K. & Mittal, R. 2014 *Synthetic Jets: Fundamentals and Applications*. CRC Press.

Raman, G., Rice, E. J. & Cornelius, D. M. 1994 Evaluation of flip-flop jet nozzles for use as practical excitation devices. *J. Fluids Eng.* **116**, 508–515.

Shtendel, T. & Seifert, A. 2014 Three-dimensional aspects of cylinder drag reduction by suction and oscillatory blowing. *Int. J. Heat Fluid Fl.* **45**, 109–127.

Tritton, D. J. 1986 *Physical Fluid Dynamics*. Oxford Science Publications.

Viets, H. 1975 Flip-flop jet nozzle. *AIAA J.* **13**, 1375–1379.

Vreman, A. W. 2004 An eddy-viscosity subgrid-scale model for turbulent shear flow: Algebraic theory and applications. *Phys. Fluids* **16**, 3670–3681.

Wassermann, F., Hecker, D., Jung, B., Markl, M., Seifert, A. & Grundmann, S. 2013 Phase-locked 3D3C-MRV measurements in a bi-stable fluidic oscillator. *Exp. Fluids* **54**, 1–15.

Wilson, J., Schatzman, D., Arad, E., Seifert, A. & Shtendel, T. 2013 Suction and pulsed-blowing flow control applied to an axisymmetric body. *AIAA J.* **51**, 2432–2446.